Torque acting on ^{252}Cf fission fragments

Guillaume Scamps[1,*]

[1]Department of Physics, University of Washington, Seattle, Washington 98195-1560, USA

Abstract.
The generation of angular momentum in the fission fragments is the subject of a renewal of interest since new experimental data [Wilson, et al.] shows that the magnitudes of the spins of the fragments are almost uncorrelated. In this proceeding, the collective potential perceived by the fission fragments is studied using static frozen Hartree-Fock calculation and the dynamic Time-Dependent Hartree-Fock. The results are in qualitative agreement with previous studies done in the case of the ^{240}Pu.

1 Introduction

Fission is the process in which one nucleus separates into two nuclei of comparable mass. An important goal of the nuclear theory [1] is to determine the properties of the fission fragments, mass, charge, energy, and spins. Experimentally the fission fragments have a large spin between 5 and 10 $\hbar$ [2]. The source of spin of the fission fragment is still an open question with different possible explanations, i) the build-up of stochastic fluctuation during the descent of the potential from the saddle to scission [3–6] ii) the quantum effect at scission [7–9] iii) the Coulomb repulsion that creates a torque on the fragments [10–12].

The two fission reactions studied here are, ^{252}Cf $\rightarrow$ ^{132}Sn + ^{120}Cd and ^{252}Cf $\rightarrow$ ^{144}Ba + ^{108}Mo. In the present approach, It is assumed that the two fragments are already formed and correspond to the ground state or a deformed configuration of the corresponding nuclei.

2 Frozen Hartree-Fock

In the Frozen-Hartree-Fock (FHF) [13, 14] calculation, the fission fragment are assumed rigid. Both fragments are put in the lattice at a distance D between their center of mass. The heavy and light fragments are oriented to form respectively an angle $\theta_{\rm H}$ and $\theta_{\rm L}$ with the fission axis. This calculation neglects more complicated shapes that are described in dynamical models such as the time-dependent Hartree-Fock plus BCS pairing model (TDHF+BCS) [15, 16] or Time-Dependent Superfluid Local Density Approximation (TDSLDA) [17]. In these models, a neck is present between the two fragments at the scission point. Nevertheless, these models respect symmetries, and so the deformed fragments at the scission are aligned with the fission axis. As we will observe with the FHF calculations, this corresponds to the arrangement that minimizes the energy. That configuration is then expected to be the most probable but fluctuations due to thermal and/or quantum effects should populate fission configurations where the fragments principle axis deviates slightly from the fission axis.

The fragments of the output channel are chosen to i) describe the main populated states ii) have different shapes to study the impact of different types of deformation on the potential. As can be seen in Table 1, the chosen fission fragment have different shapes: spherical for the ^{132}Sn, quadrupole for the ^{120}Cd and ^{108}Mo and an octupole ^{144}Ba. The ^{108}Mo also shows a hexadecapole deformation. These two output channels belong to the channels that are enough populated to be experimentally studied [18].

Table 1. The deformations and rigid moments of inertia of the four nuclei examined in this study. The rigid moment of inertia in unit of [$\hbar^2$/MeV] is obtained on an axis perpendicular to the main deformation axis of the nucleus. The excitation energy of the deformed state is also shown in the case of the ^{120}Cd which is not in its ground state.

Nuc.	β_2	β_3	β_4	E^* [MeV]	$I_{\rm Rigid}$
^{132}Sn	0.	0.	0.	0	50.0
^{120}Cd	0.42	0.	0.08	4.4	51.5
^{144}Ba	0.22	0.16	0.15	0	63.1
^{108}Mo	0.58	0.	0.25	0	46.1

The calculations are done in a lattice with a mesh constant dx = 0.8 fm. All calculations of the proceeding are obtained with the Sly4d functional [19]. The fragments are obtained with the Sky3d code [20] on a cubic lattice with $L_x = L_y = L_z$=24 fm. The fragments are then placed on an extended lattice with Lx = 60 fm. The energy of the total system is then computed, and the radial potential is defined as,

$$V = E_{FHF}(\theta, D) - E_{FHF}(\theta = 0, D). \quad (1)$$

In the present static study, the calculation are limited to only one non-zero orientation angle at a time. The angle of

*e-mail: gscamps@uw.edu

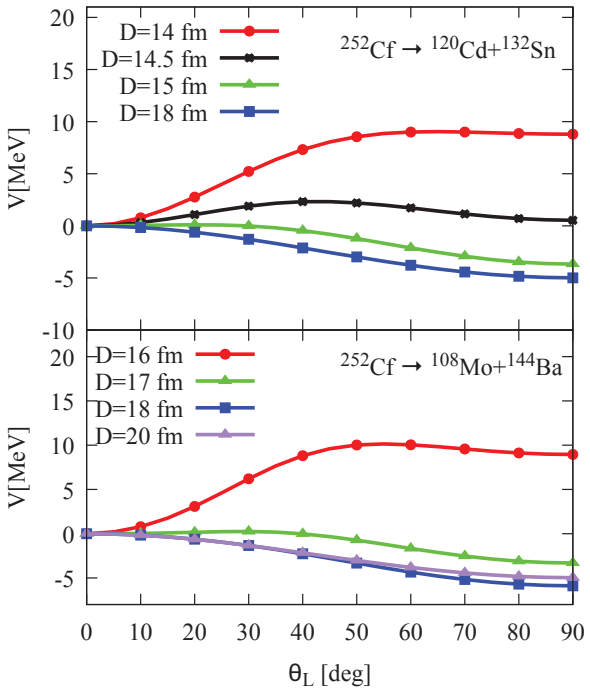

Figure 1. Frozen Hartree-Fock radial potential as a function of the orientation angle of the light fragment for different separation between the fission fragments. The heavy fragment is aligned with the fission axis θ_H=0.

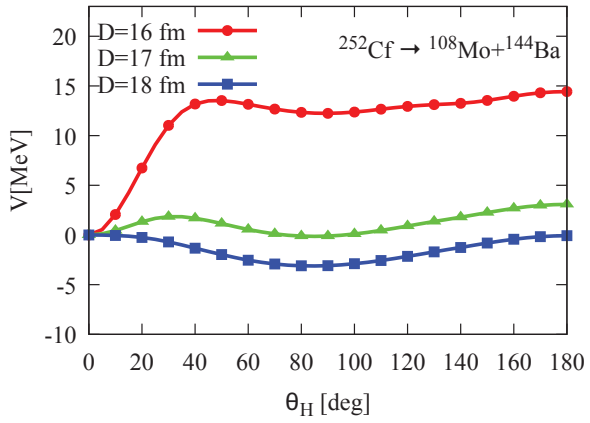

Figure 2. Same as Fig. 1 for the heavy fragment. This fragment being pear-shaped deformed the x-axis of the figure vary from 0 (the heavy fragment point to the other fragment) to 180 degrees. The light fragment is aligned with the fission axis θ_L=0.

the other fragment is assumed to be zero. More complex effects of the correlation between the angles have been studied in Ref. [21] and show a small impact of the correlations. At small angles, the principal impact of the orientation on the energy is then the sum of each fragment contribution. In Fig. 1, the angular potential is shown for the heavy fragment. In both case, the potential show similar behavior, at small distances the fragments can touch each other, and the attractive nucleus-nucleus potential favors the θ=0 configuration. When the distance increases, the nuclear effect drop-off, and the Coulomb potential dominates. The Coulomb energy favors configurations at 90 degrees, then the lowest configuration changes during the scission process from 0 degrees to 90 degrees.

From this static picture, we can estimate the evolution of the system, the fragments are first oriented in the 0 degrees configuration. Beyond the classical approximation, it is expected that statistical or quantum fluctuations will make the fragments deviate from the exact 0 degrees configuration. Then once the system passes the scission point, the 0 degrees configuration become unstable. This lead to a rotational acceleration of the fission fragments due to the Coulomb torque.

3 Time-dependent Hartree-Fock

To describe microscopically that evolution, we solve the TDHF equations with the initial configuration described previously i.e the center of mass of the fragments are at a distance D and oriented with an angle $\theta_{L,R}$. The evolution of the one-body density is shown by a contour plot, in Fig. 3 and 4 panel (a), (b), and (c). Initially oriented at an angle of 25 degrees and at a distance for which there is a nucleus-nucleus interaction (14 fm and 16 fm respectively for the ^{252}Cf → ^{132}Sn + ^{120}Cd and ^{252}Cf → ^{144}Ba + ^{108}Mo channels). The static potential described in the previous section and the additional contribution due to the neck, makes the fragment rotate.

During the evolution, for each fragment, the local total angular momentum is calculated as,

$$\mathbf{J}(\mathbf{r}) = \hbar \sum_{i,\mathbf{F}} \langle \Phi_i(\mathbf{r})| \left((\hat{\mathbf{r}} - \mathbf{r}_{\rm cm}) \times (\hat{\mathbf{p}} - \mathbf{p}_{\rm cm}) + \hat{\mathbf{s}}\right) \; \mathbf{\Theta_F} |\Phi_i(\mathbf{r})\rangle, \tag{2}$$

With $\mathbf{r}_{\rm cm}$ and $\mathbf{p}_{\rm cm}$ respectively the position and impulsion of the fragments. The sum over i includes all occupied protons and neutrons wave function $|\Phi_i(\mathbf{r})\rangle$. The Heaviside function $\mathbf{\Theta_F}$ is the projector operator on the half-space containing the fragment $\mathbf{F}$. That operator reveals how the angular momentum is distributed inside the fragment. The distribution of a rigid rotor would behave as $r\rho(\mathbf{r})$.

That quantity is shown on the three first panels of Fig. 3 and 4. It shows that the fragment deviates from the rigid rotor model. The fragments being excited, different modes of vibrations are populated.

The integral of $\mathbf{J}(\mathbf{r})$ leads to the total angular momentum of the fragments. its evolution as well as the contribution of the protons and neutrons are shown on panel (d) of Fig. 3 and 4. The evolution is strongly dependent on the shapes of the fragments. In the initially spherical ^{132}Sn, the interaction with the other fragment breaks the spherical symmetry and so enables the generation of a small angular momentum. Both ^{120}Cd and ^{108}Mo have a large quadrupole deformation. They see their angular momentum increase rapidly due to the restoring torque. After separation, the angular momentum decreases slightly due to the Coulomb torque. The Coulomb torque can either increase or decrease the angular momentum depending on

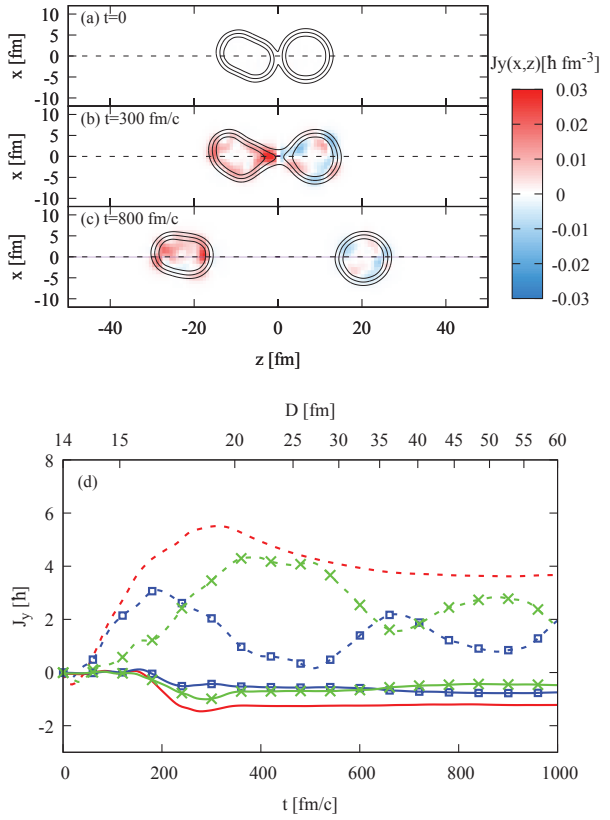

Figure 3. Panel (a-c) Snapshot of the contour density (solid lines) as a function of time for the fission reaction ^{252}Cf → ^{132}Sn + ^{120}Cd. The colors show the local angular momentum. The calculation starts at 14 Fm. The light fragment is oriented at an angle θ_L=25°. Panel (d) shows the evolution as a function of time and as a function of the distance D the total spin of the heavy (solid line) and light (dashed line) fragments. For both fragments, the contribution of protons and neutrons are shown respectively by blue squares and green crosses.

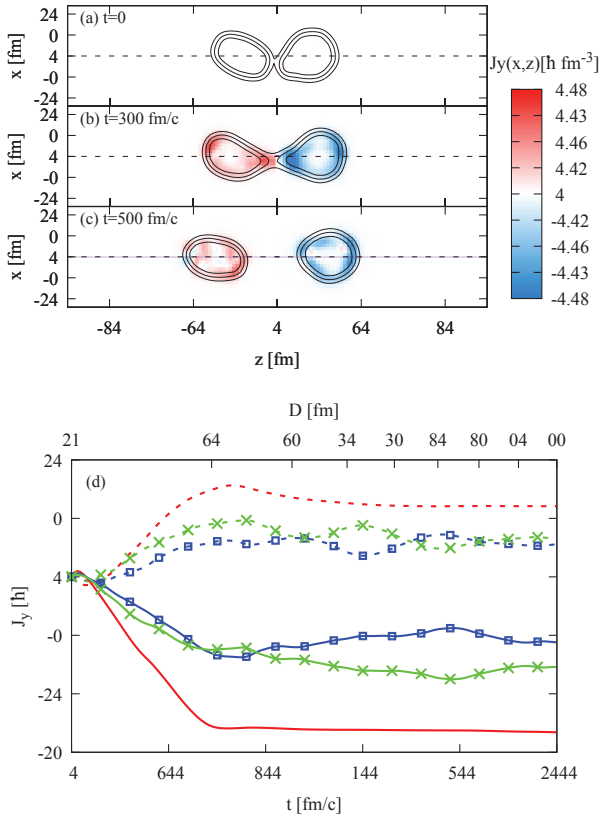

Figure 4. Same as Fig. 3 for the reaction ^{252}Cf → ^{144}Ba + ^{108}Mo. The calculation starts at a distance D=16 fm.

the orientation and direction of the angular momentum of the fragments. The pear-shaped ^{144}Ba has the largest final angular momentum. This result is coherent with the static picture since the potential for the heavy fragment (see Fig. 2) is stiffer than for the light fragment (See Fig. 1(b)). This confirms the finding in Ref. [22] that the octupole deformation increases substantially the generation of angular momentum.

A surprising effect, already shown in Ref. [21], is the large transfer of angular momentum between protons and neutrons visible in panel (d) of Fig. 3 and 4. An extreme case is found in the ^{120}Cd fragment. The angular momentum is generated initially in the protons but at t = 500 fm/c the angular momentum is completely dominated by the neutrons.

4 Conclusion

The present results concerning the fission of ^{252}Cf are in qualitative agreement with Ref. [21] which was done for two ^{240}Pu fission channels. A strong restoring force takes place at scission, which creates an angular momentum in the fission fragments if the orientation deviates from θ=0. The goal of the present study is not to obtain results that can be compared to experimental results since the final angular momentum in the fragment depends strongly on the initial angle. Nevertheless, the present FHF results can be used to determine the final angular momentum using the collective hamiltonian model [22].

Acknowledgements

The funding from the US DOE, Office of Science, Grant No. DE-FG02-97ER41014 is greatly appreciated. This research used resources of the Oak Ridge Leadership Computing Facility, which is a U.S. DOE Office of Science User Facility supported under Contract No. DE-AC05-00OR22725.

References

[1] M. Bender, *et. al.*, J. Phys. G: Nucl. Part. Phys. **47** 113002 (2020).
[2] J. B. Wilhelmy, E. Cheifetz, R. C. Jared, S. G. Thompson, H. R. Bowman, and J. O. Rasmussen, Phys. Rev. C **5**, 2041 (1972).
[3] L. G. Moretto and R. P. Schmitt, Phys. Rev. C **21**, 204 (1980).
[4] T. Døssing and J. Randrup, Nuclear Physics A **433**, 215-279 (1985).

[5] J. Randrup and R. Vogt, Phys. Rev. Lett. **127**, 062502 (2021).
[6] J. Randrup, T. Døssing, and R. Vogt, Phys. Rev. C **106**, 014609 (2022).
[7] I. N. Mikhailov and P. Quentin, Physics Letters B **462**, 7–13 (1999).
[8] L. Bonneau, P. Quentin, and I. N. Mikhailov, Phys. Rev. C **75**, 064313 (2007).
[9] T. M. Shneidman, G. G. Adamian, N. V. Antonenko, S. P. Ivanova, R. V. Jolos, and W. Scheid, Phys. Rev. C **65**, 064302 (2002).
[10] Marvin M. Hoffman, Phys. Rev. **133**, B714 (1964).
[11] K. Alder, and A. Winther, *Electromagnetic excitation: Theory of Coulomb excitation with heavy ions* (North-Holland, Amsterdam) (1975).
[12] G.F. Bertsch, arXiv:1901.00928 [nucl-th] (2019).
[13] C. Simenel, A. S. Umar, K. Godbey, M. Dasgupta, and D. J. Hinde, Phys. Rev. C **95**, 031601(R) (2017).
[14] A. S. Umar, C. Simenel, and K. Godbey, Phys. Rev. C **104**, 034619 (2021).
[15] G. Scamps, C. Simenel, D. Lacroix, Phys. Rev. C **92**, 011602(R) (2015).
[16] G. Scamps and C. Simenel, Nature volume **564**, 382-385 (2018).
[17] A. Bulgac, P. Magierski, K. J. Roche, and I. Stetcu, Phys. Rev. Lett. **116**, 122504 (2016).
[18] J.N. Wilson, D. Thisse, M. Lebois, et al. Nature, **590**, 566–570 (2021).
[19] K.-H. Kim, T. Otsuka, and P. Bonche, J. Phys. G **23**, 1267 (1997).
[20] B. Schuetrumpf, P.-G. Reinhard, P.D. Stevenson, A.S. Umar, and J.A. Maruhn, Comp. Phys. Comm. **229**, 211-213 (2018).
[21] G. Scamps, Phys. Rev. C **106**, 054614 (2022).
[22] G. Scamps and G. Bertsch, arXiv:2302.07792 [nucl-th] (2023).